sures between 0 and 10 GPa were applied with a diamond anvil cell (DAC) and were measured with standard ruby fluorescence techniques to ±0.2 GPa (*15*).
13. C. B. Murray, D. J. Norris, M. G. Bawendi, *J. Am. Chem. Soc.* **115**, 8706 (1993).
14. X. G. Peng, J. Wickham, A. P. Alivisatos, *J. Am. Chem. Soc.* **120**, 5343 (1998).
15. For a review of ruby measurements, see J. D. Barnett, S. Block, G. J. Piermari, *Rev. Sci. Instrum.* **44**, 1 (1973).
16. The four-coordinate structure is a direct band-gap semiconductor with an electronic absorbance peak in the visible spectrum, whereas the six-coordinate structure is an indirect band-gap semiconductor and has a featureless spectrum [see also (*25*)]. Light from a tungsten-halogen source was sent through a sample loaded in the DAC. The transmitted light was directed into a spectrometer and detected with a liquid N_2–cooled charge-coupled device camera. Static temperature control to 510 K was achieved by placing the cell in a resistively heated ceramic oven and was measured with a thermocouple in contact with the diamond. Remote control of the pressure in the DAC by a computer-controlled stepper motor made it possible to measure relatively fast transition times on the order of seconds.
17. M. G. Evans, M. Polanyi, *Trans. Faraday Soc.* **1935** (1935).
18. X. Y. Li, R. Jeanloz, *Phys. Rev. B* **36**, 474 (1987).
19. F. P. Bundy, *Proc. K. Ned. Akad. Wet. Ser. B Phys. Sci.* **72**, 302 (1969).
20. J. W. Christian, *The Theory of Transformations in Metals and Alloys*, Part 1, Equilibrium and General Kinetic Theory (Pergamon, Oxford, New York, 1965).
21. L. E. Brus, J. A. W. Harkless, F. H. Stillinger, *J. Am. Chem. Soc.* **118**, 4834 (1996).
22. J. Osugi, K. Shimizu, T. Nakamura, A. Onodera, *Rev. Phys. Chem. Jpn.* **36**, 59 (1966).
23. D. A. Porter, K. E. Easterling, *Phase Transformations in Metals and Alloys* (Chapman and Hall, London, ed. 2, 1992).
24. Increasing activation energies of 0.5, 1.2, 1.7, and 2.4 eV/nanocrystal were reported for CdSe nanocrystal diameters of 20, 27, 34, and 43 Å, respectively, in the forward transition; see (*25*).
25. C. C. Chen, A. B. Herhold, C. S. Johnson, A. P. Alivisatos, *Science* **276**, 398 (1997).
26. S. Takeuchi, K. Suzuki, K. Maeda, H. Iwanaga, *Philos. Mag. A.* **50**, 171 (1984).
27. R. S. Berry, B. M. Smirnov, *J. Chem. Phys.* **113**, 728 (2000).
28. Above a temperature limit of 575 K, interparticle diffusion can occur and the nanocrystals are no longer isolated and distinct particles; see (*29*).
29. A. B. Herhold, thesis, University of California, Berkeley (1997).
30. L. D. Landau, E. Lifshitz, *Statistical physics*, J. B. Sykes, M. J. Kearsley, Eds. (Pergamon, New York, 1980).
31. L. Néel, *Compt. Rend. Acad. Sci. Paris* **228**, 664 (1949).
32. W. F. Brown, *Ann. NY Acad. Sci.* **147**, 461 (1969).
33. H. L. Richards, M. Kolesik, P.-A. Lindgard, *Phys. Rev. B* **55**, 11521 (1997).
34. M. J. O'Shea, H. Jiang, P. Perera, H. H. Hamdeh, *J. Appl. Phys.* **87**, 6137 (2000).
35. T. Chang, J.-G. Zhu, J. H. Judy, *J. Appl. Phys.* **73**, 6716 (1993).
36. We used magnetization of 0.15 A·m^2 per gram in 100 Å Fe-Co crystals and the permeability in free space for hysteresis loops taken at 76 K; see (*37*).
37. F. E. Luborsky, T. O. Paine, *J. Appl. Phys.* **31**, S68-S70 (1960).
38. The large structural hysteresis area is consistent with the smearing calculation, indicating that experimental temperatures are small relative to the thermal energy of the structural hysteresis. The energy disparity between the transitions is related to the fact that superparamagnetism (free-energy barrier is on the order of thermal energy) often occurs in magnetic nanocrystals, while the structural analog has yet to be observed in nanocrystals. The disparity is also quantitatively consistent with the 10-year relaxation time at the thermodynamic pressure in 25 Å CdSe nanocrystals, which occurs in a magnetic transition in nanocrystals over 200 Å in diameter; see (*39*).
39. H. J. Richter, *J. Phys. D Appl. Phys.* **32**, R147 (1999).
40. K. Jacobs *et al.*, in preparation.
41. We thank J. Wickham, R. Jeanloz, and G. Inger for helpful discussions and E. Granlund and H. Gretch for machining work on the DAC. This work was supported by the director, Office of Energy Research, Office of Science, Division of Materials Sciences, of the U. S. Department of Energy, and the Air Force Office of Scientific Research, Air Force Material Command, U.S. Air Force. We used the facilities of the National Center for Electron Microscopy for the electron microscope images.

19 June 2001; accepted 9 August 2001

Antibody Catalysis of the Oxidation of Water

Paul Wentworth Jr.,[1] Lyn H. Jones,[1] Anita D. Wentworth,[1] Xueyong Zhu,[1] Nicholas A. Larsen,[1] Ian A. Wilson,[1] Xin Xu,[2] William A. Goddard III,[2] Kim D. Janda,[1] Albert Eschenmoser,[1,3] Richard A. Lerner[1]

Recently we reported that antibodies can generate hydrogen peroxide (H_2O_2) from singlet molecular oxygen ($^1O_2$*). We now show that this process is catalytic, and we identify the electron source for a quasi-unlimited generation of H_2O_2. Antibodies produce up to 500 mole equivalents of H_2O_2 from $^1O_2$*, without a reduction in rate, and we have excluded metals or Cl^- as the electron source. On the basis of isotope incorporation experiments and kinetic data, we propose that antibodies use H_2O as an electron source, facilitating its addition to $^1O_2$* to form H_2O_3 as the first intermediate in a reaction cascade that eventually leads to H_2O_2. X-ray crystallographic studies with xenon point to putative conserved oxygen binding sites within the antibody fold where this chemistry could be initiated. Our findings suggest a protective function of immunoglobulins against $^1O_2$* and raise the question of whether the need to detoxify $^1O_2$* has played a decisive role in the evolution of the immunoglobulin fold.

Antibodies, regardless of source or antigenic specificity, generate H_2O_2 from $^1O_2$*, thereby potentially aligning recognition and killing within the same molecule (*1*). Given the potential chemical and biological importance of this observation, the mechanistic basis of this process and its structural location within the antibody have been investigated. Together these studies reveal that antibodies, in contrast to other proteins, may catalyze an unprecedented set of chemical reactions between water and $^1O_2$*.

Long-term ultraviolet (UV) irradiation studies reveal that antibody-mediated H_2O_2 production is much more efficient than for non-immunoglobulin proteins (Fig. 1A). Typically antibodies exhibit linearity in H_2O_2 formation for up to 40 mole equivalents of H_2O_2 before the rate begins to decline asymptotically (Fig. 1B). Non-immunoglobulin proteins display a short burst of H_2O_2 production followed by quenching as photo-oxidation occurs (Fig. 1A). Also, antibodies can resume photoproduction of H_2O_2 at the same initial rate if H_2O_2 is removed by catalase (Fig. 1C). Thus, H_2O_2 reversibly inhibits its own formation. The apparent median inhibitory concentration (IC_{50}) was estimated as 225 μM (Fig. 1E). Antibody-mediated photoproduction of H_2O_2 can also be saturated with molecular oxygen (apparent Michaelis-Menten constant for oxygen = 187 μM) (*1*), which, when allied with the H_2O_2 inhibition aspect, suggests a binding site process.

Even after 10 cycles of UV irradiation followed by addition and removal of catalase (which generates ~500 mole equivalents of H_2O_2), only a slight reduction (5%) is seen in the initial rate. Beside antibodies, the only other protein that we have found thus far to generate H_2O_2 catalytically is the αβ T cell receptor (αβTCR) (Fig. 1D), which shares a similar arrangement of its immunoglobulin fold domains with antibodies (*2*). However, possession of this structural motif does not necessarily confer an H_2O_2-generating ability on proteins; β_2-microglobulin, although a member of the immunoglobulin superfamily (*3*), does not generate H_2O_2.

The antibody structure is remarkably inert to the oxidizing effects of H_2O_2. SDS–polyacrylamide gel electrophoresis of antibody samples after UV irradiation under standard conditions for 8 hours revealed no significant fragmenta-

[1]Departments of Chemistry and Molecular Biology and Skaggs Institute for Chemical Biology, Scripps Research Institute, 10550 North Torrey Pines Road, La Jolla, CA 92037, USA. [2]Materials and Process Simulation Center, Division of Chemistry and Chemical Engineering (MC 139-74), California Institute of Technology, Pasadena, CA 91125, USA. [3]Laboratorium für Organische Chemie, Eidgenössische Technische Hochschule (ETH) Zürich, Universitätstrasse 16, CH-8092 Zürich, Switzerland.

tion or agglomeration of the antibody. Also, the native and H_2O_2-treated structures of murine Fab 4C6 (*4, 5*) are superimposable at the level of side-chain positions, reinforcing the evidence of stability of the antibody fold in the presence of H_2O_2 (Fig. 2).

The photoactivity of the antibody appears to be driven through tryptophan (Trp) absorbance. An action spectrum of the antibody-mediated photoproduction of H_2O_2 and the corresponding absorbance spectrum of the antibody protein for wavelengths from 260 to 320 nm are virtually superimposable (Fig. 3). The maximal efficiency of H_2O_2 production occurs at the same wavelength as the UV absorbance maxima of Trp in proteins (~280 nm). We probed the efficiency of H_2O_2 production by horse immunoglobulin G (IgG) as a function of the efficiency of $^1O_2$* formation via $^3O_2$ sensitization with hematoporphyrin IX [quantum yield of singlet oxygen formation (ϕ_Δ) = 0.22 in phosphate buffer (pH 7.0) and visible light (*6, 7*)]. For every 275 ± 25 mole equivalents of $^1O_2$* generated by sensitization, 1 mole equivalent of H_2O_2 was generated by the antibody molecule.

The conversion of $^1O_2$* to H_2O_2 requires two mole equivalents of electrons, and we have generated >500 equivalents of H_2O_2 per equivalent of antibody molecule with no notable reduction in rate. Thus, the ultimate electron source clearly cannot be the antibody itself. Both as an individual amino acid and as a constituent of proteins, Trp is particularly sen-

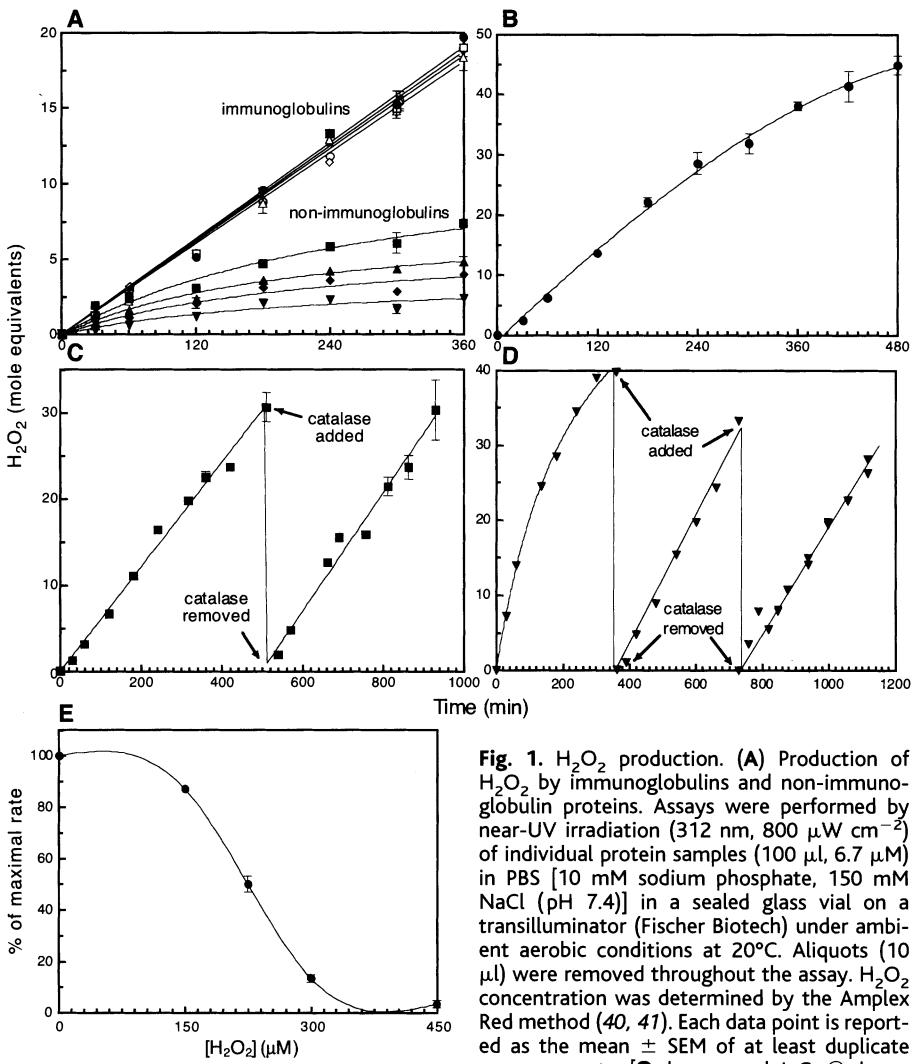

Fig. 1. H_2O_2 production. (**A**) Production of H_2O_2 by immunoglobulins and non-immunoglobulin proteins. Assays were performed by near-UV irradiation (312 nm, 800 μW cm^{-2}) of individual protein samples (100 μl, 6.7 μM) in PBS [10 mM sodium phosphate, 150 mM NaCl (pH 7.4)] in a sealed glass vial on a transilluminator (Fischer Biotech) under ambient aerobic conditions at 20°C. Aliquots (10 μl) were removed throughout the assay. H_2O_2 concentration was determined by the Amplex Red method (*40, 41*). Each data point is reported as the mean ± SEM of at least duplicate measurements: [●, human polyIgG; ○, horse polyIgG; □, sheep polyIgG; ▽, murine mIgG (WD1-6G6); △, human polyIgM; ◇, murine mIgG (92H2); ■, β-galactosidase (β-gal); ▲, chick ovalbumin; ▼, α-lactalbumin; ◆, bovine serum albumin]. (**B**) Long-term production of H_2O_2 by sheep polyIgG (6.7 μM, 200 μl). Near-UV irradiation for 8 hours in PBS in a sealed well of a 96-well quartz plate, H_2O_2 concentration was measured as described in (A). (**C**) A solution of murine mIgG PCP21H3 (6.7 μM, 200 μl) was irradiated in PBS in a sealed well of a 96-well quartz plate for 510 min. The H_2O_2 was assayed by the Amplex Red assay and then destroyed by addition of catalase (10 mg, 288 mU) immobilized on Eupergit C. The catalase was removed by filtration, and the antibody solution was reirradiated for 420 min; rate (0 to 510 min) = 0.368 μM min^{-1} (r^2 = 0.998); rate (511 to 930 min) = 0.398 μM min^{-1} (r^2 = 0.987). This profile of continued linear production of H_2O_2 after catalase-mediated destruction of H_2O_2 is conserved for all antibodies assayed. (**D**) A solution of TCRαβ (6.7 μM, 200 μl) was irradiated as described in (C) for periods of 360, 367, and 389 min. The H_2O_2 generated during each irradiation was assayed and destroyed as described in (C). The curvature in the progress curve above 30 mole equivalents conforms to the expected inhibition by H_2O_2 (see below); rate (361 to 727 min) = 0.427 μM min^{-1} (r^2 = 0.987); rate (728 to 1117 min) = 0.386 μM min^{-1} (r^2 = 0.991). (**E**) Determination of IC_{50} of H_2O_2 on the photoproduction of H_2O_2 by horse polyIgG. A solution of horse IgG (6.7 μM) was incubated with varying concentrations of H_2O_2 (0 to 450 μM), and the initial rate of H_2O_2 formation was measured as described in (A). The graph is a plot of rate of H_2O_2 formation versus H_2O_2 concentration and reveals an IC_{50} of 225 μM.

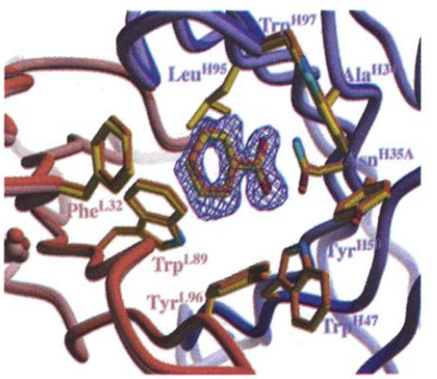

Fig. 2. Superposition of the 4C6 combining site with and without H_2O_2 demonstrates that even the side-chain conformations within the binding site are preserved (light- and dark-colored side chains, pink for the light chains and blue for the heavy chains, correspond to + and – H_2O_2, respectively). Moreover, clear electron density for a benzoic acid ligand underscores that the binding properties of Fab 4C6 remain unaltered in 3 mM H_2O_2. The electron density map is a $2F_{obs} - F_{calc}$ σ-weighted map contoured at 1.5σ. (Figure was generated with Bobscript.) Details of this structure will be presented elsewhere.

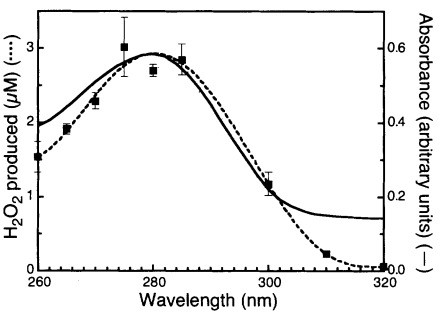

Fig. 3. Absorbance spectrum (—) and action spectrum (–■–) of horse polyIgG between 260 and 320 nm. The absorbance spectrum was measured on a diode array HP8452A spectrophotometer (maximum absorbance, 280 nm). The action spectrum was measured by placing an antibody solution [6.7 μM in PBS (pH 7.4)] in a quartz tube in the light beam produced by a xenon arc lamp and monochromator of an SLM spectrofluorimeter for 1 hour. H_2O_2 concentration was measured by the Amplex Red assay (*40, 41*).

sitive to near-UV irradiation (300 to 375 nm) under aerobic conditions, owing to its conversion to *N*′-formylkynurenine (NFK), which is a particularly effective near-UV (λ_{max} = 320 nm) photosensitizer (*8*). However, photo-oxidation of Trp (the free amino acid) is accompanied by substoichiometric production of H_2O_2 (~0.5 mole equivalents) during near-UV irradiation (Fig. 4A) (*9*), and the most efficient non-immunoglobulin protein at H_2O_2 photoproduction, β-galactosidase, generates only 7 mole equivalents of H_2O_2 from its 39 Trp residues (*10*) (Fig. 1A). Even if every photo-oxidizable residue (Trp, Tyr, Cys, Met, and His) were consumed, this could not account for 500 mole equivalents of H_2O_2 (*7*).

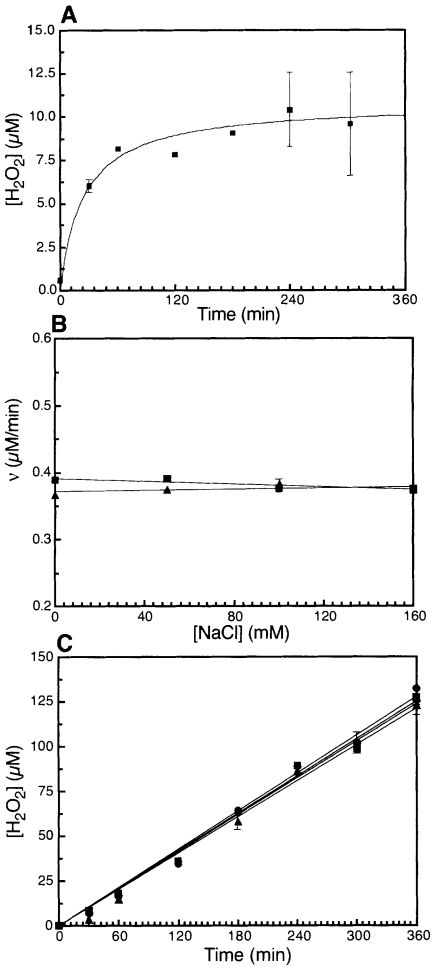

Fig. 4. (**A**) Production of H_2O_2 by Trp (20 μM). The conditions and assay procedures were as described in Fig. 1A. (**B**) Effect of [Cl^-] on antibody-mediated photoproduction of H_2O_2. A solution of sheep polyIgG (■, 6.7 μM, 200 μl) or horse polyIgG (▲, 6.7 μM, 200 μl) in PB (pH 7.4) was lyophilized to dryness and then dissolved in either deionized water or NaCl (aq.) such that the final [Cl^-] was 0 to 160 mM. The samples were then irradiated, in duplicate, in sealed glass vials on a transilluminator (800 μW cm^{-2}) under ambient aerobic conditions at 20°C. Aliquots (10 μl) were removed throughout the assay; H_2O_2 concentration was determined by the Amplex Red assay (*40, 41*). The rate of H_2O_2 formation, *v*, is plotted as the mean ± SEM versus [NaCl] for each antibody sample. (**C**) Effect of dialysis into EDTA-containing buffers on antibody-mediated photoproduction of H_2O_2. The photoproduction of H_2O_2 by two antibody preparations, mouse mIgG PCP21H3 and horse polyIgG, were compared before and after dialysis into PBS containing EDTA (20 mM). The conditions and assay procedures were as described in Fig. 1A. Each data point is reported as the mean ± SEM of at least duplicate measurements (●, murine mIgG PCP21H3 before dialysis; ■, murine mIgG PCP21H3 after dialysis; ▲, horse polyIgG before dialysis; ◆, horse polyIgG after dialysis).

The next most likely source is Cl^-, which is a suitable electron source for photoproduction of H_2O_2 via a triplet-excited state of an anthraquinone (*11*). We thus investigated the potential of Cl^- [present at 150 mM in phosphate-buffered saline (PBS)] as a reducing equivalent. However, the rate of H_2O_2 production by immunoglobulins was independent of [Cl^-] in the range 0 to 160 mM (Fig. 4B).

We also considered the possible role of metal ions. Although such ions could hardly be sufficiently abundant in antibodies to serve as an electron source, trace amounts of them might play a central role as catalytic redox centers. The following experiments allowed us to rule out the implication of trace metals in this process: (i) The rate of antibody-mediated photoproduction of H_2O_2 is unchanged before and after exhaustive dialysis of antibody samples with EDTA-containing buffer (Fig. 4C). (ii) After EDTA treatment of antibody samples, inductively coupled plasma–atomic emission spectroscopy (ICP-AES) reveals the presence of remaining trace metal ions in amounts far less than 1 part per million (*7*). (iii) For a trace metal to be implicated in this reaction, it must be common to all antibodies because all antibodies assayed have this intrinsic ability. It is generally accepted that metal binding is not an implicit feature of antibodies; this idea is consistent with our own analysis of antibody crystals as well as the ~300 antibody structures available in the Brookhaven database.

All of our observations thus far pointed toward an electron source that does not deactivate the protein catalyst, could account for the high turnover numbers, and hence is quasi-unlimited. Our attention thus turned to a broader consideration of the chemical potential of $^1O_2$*.

The known chemistry of $^1O_2$* (*12*) can be conceptualized as the chemistry of the super-electrophile "dioxa-ethene." So we considered that a molecule of water may, in the presence of an antibody, add as a nucleophile to $^1O_2$* and form H_2O_3 as an intermediate. Water, in becoming oxidized to H_2O_2, would fulfill the role of the electron source.

Isotope experiments were undertaken to determine the source of oxygen found in the H_2O_2. Contents of $^{16}O/^{18}O$ in H_2O_2 were measured by modification of a standard H_2O_2 detection method: reduction with tris(carboxyethyl)phosphine (TCEP) (*13*) followed by mass-spectral analysis of the corresponding phosphine oxides (Fig. 5).

In the presence of oxygen, UV irradiation of antibodies leads to oxygen incorporation from water into H_2O_2 (*7*). The relative abundance of the $^{16}O/^{18}O$ ratio observed in the mass spectra of the phosphine oxide after irradiation of sheep polyclonal IgG (polyIgG) under conditions of saturating $^{16}O_2$ concentration in a solution of $H_2{}^{18}O$ (98% ^{18}O) phosphate buffer (PB) was (2.2 ± 0.2):1 (Fig. 5A) (*7*). When the converse experiment was performed with an ^{18}O-enriched molecular oxygen mixture (90% ^{18}O) in $H_2{}^{16}O$ PB, the reverse ratio [1:(2.0 ± 0.2)] was observed (Fig. 5B) (*14*). These ratios exhibit good reproducibility (±10%, n = 10) (*15*) and were found for all antibodies studied (*16*).

The following control experiments were performed. First, under conditions of $^{16}O_2$ and $H_2{}^{16}O$, irradiation of horse polyIgG generates $H_2{}^{16}O_2$ (Fig. 5C). No incorporation of ^{18}O occurs when $H_2{}^{16}O_2$ (400 μM in PB, pH 7.0) itself is irradiated for 4 hours in $H_2{}^{18}O$. Thus, ^{18}O incorporation into H_2O_2 does not occur either by an acid-catalyzed exchange with water or by a mechanism that involves homolytic cleavage of $H_2{}^{16}O_2$ and recombination with $H^{18}O^{\bullet}$ from water. To investigate the possibility that antibodies may catalyze both the production of $H_2{}^{16}O_2$ and its acid-catalyzed exchange with $H_2{}^{18}O$, we determined the isotopic exchange of $H_2{}^{16}O_2$ (200 μM) in $H_2{}^{18}O$ (98% ^{18}O) PB in the presence of sheep polyIgG (6.7 μM) after UV irradiation under an inert atmosphere. Only a trace of incorporation of ^{18}O into $H_2{}^{16}O_2$ (<1%) was observed (Fig. 5D) (*17*).

The thermodynamic balance between reactants and products for the oxidation of H_2O by $^1O_2$* (heat of reaction ΔH_r = +28.1 kcal/mol, Eq. 1a) (*18*) demands a stoichiometry in which more than one molecule of $^1O_2$* must participate per molecule of oxidized water during its conversion into two molecules of H_2O_2. This stoichiometry assumes that no further light energy apart from that involved in the production of singlet from triplet oxygen is participating in the process. Qualitative chemical reasoning on hypothetical mechanistic pathways, together with thermodynamic considerations, makes the overall stoichiometries likely to be those shown in Eqs. 1b or 1c (heats of formation ΔH_r° are reported in kcal/mol):

$$^1O_2^* + 2H_2O \rightarrow 2H_2O_2 \quad \Delta H_r^\circ = 28.1 \quad (1a)$$

$$2\,^1O_2^* + 2H_2O \rightarrow 2H_2O_2 + {}^3O_2 \quad \Delta H_r^\circ = 5.6 \quad (1b)$$

$$3\,^1O_2^* + 2H_2O \rightarrow 2H_2O_2 + 2\,^3O_2 \quad \Delta H_r^\circ = -16.9 \quad (1c)$$

A recent report of a transition metal–catalyzed conversion of $^1O_2$ and water into H_2O_2 via a tellurium-mediated redox process (*19*) provides

experimental evidence for a process in which $^1O_2$* and H_2O can be converted into H_2O_2. Hence, the energetic demands of this process can be overcome. At the heart of our considerations of a mechanism for the antibody-mediated photo-oxidation process is the hypothesis that addition of a water molecule to a molecule of $^1O_2$* forms H_2O_3 as the first intermediate on the way to H_2O_2. The antibody's function as a catalyst would have to be the supply of a specific molecular environment that would stabilize this critical intermediate relative to its reversible formation and/or would accelerate the consumption of the intermediate by channeling its conversion to H_2O_2. An essential feature of such an environment might consist of a special constellation of organized water molecules at an active site conditioned by an antibody-specific surrounding.

Although H_2O_3 has not yet been detected in biological systems, its chemistry in vivo has been a source of considerable speculation, and its in vitro properties have been the subject of numerous experimental and theoretical treatments (*20*–*27*). Koller and Plesnicar have shown that H_2O_3 reductively generated from ozone decomposes into H_2O and $^1O_2$* in a process catalyzed by a water molecule (*26*). Applying the principle of microscopic reversibility, we surmised that one or more molecules of water should also catalyze the reverse reaction. To delineate plausible reaction routes and energetics of such a process, we used first-principles quantum chemical (QC) methods [B3LYP (*7*)]:

$$\underset{0.0}{H_2O} + \underset{}{^1O_2{}^*} \rightarrow \underset{64.7}{TS} \rightarrow \underset{12.0}{H_2O_3} \qquad (2a)$$

$$\underset{0.0}{2H_2O} + \underset{}{^1O_2{}^*} \rightarrow \underset{-7.5}{[H_2O\text{-}H_2O\text{-}^1O_2{}^*]} \rightarrow \underset{31.2}{TS} \rightarrow$$

$$\underset{4.6}{[H_2O_3 - H_2O]} \rightarrow \underset{12.0}{H_2O_3} + H_2O$$

(2b)

$$\underset{0.0}{3H_2O} + \underset{}{^1O_2{}^*} \rightarrow \underset{-17.7}{[H_2O\text{-}H_2O\text{-}H_2O\text{-}^1O_2{}^*]} \rightarrow \underset{12.0}{TS} \rightarrow$$

$$\underset{-4.8}{[H_2O_3\text{-}H_2O\text{-}H_2O]} \rightarrow \underset{12.0}{H_2O_3} + 2H_2O$$

(2c)

In these equations, all energetics are in kcal/mol. The direct reaction of water and $^1O_2$* to give H_2O_3 is quite unfavorable, with an activation barrier of 64.7 kcal/mol (Eq. 2a). However, with the addition of a second or third water molecule, we find a concerted process that decreases the activation barrier to 31.2 kcal/mol and 12.0 kcal/mol, respectively. Indeed, these additional waters play a catalytic role (in Eq. 2b, the H of the second water goes to the product HOOOH, simultaneous with the H of the first water replacing it). Note that the reverse reaction in Eqs. 2b and 2c has a barrier of only 19.2 kcal/mol or 0 kcal/mol, respectively, which suggests that H_2O_3 is not stable in bulk water or water-rich systems. Thus, we expect that the best site within the antibody structure for producing and using H_2O_3 would be one in which there are localized waters and water dimers next to hydrophobic regions without such waters.

We note that a 2.2:1 $^{16}O/^{18}O$ incorporation ratio would coincide exactly with the value predicted for certain mechanisms in which two molecules of $^1O_2$* and two molecules of H_2O are transformed into two molecules of H_2O_2 and one molecule of O_2 (which would have to be $^3O_2$ for thermodynamic reasons). An example is a second-order nucleophilic substitution (S_N2-type disproportionation) of two molecules of H_2O_3 into H_2O_4 and H_2O_2, followed by the decomposition of the former into H_2O_2 and $^3O_2$ (*28*). Although our experimental evidence leads us to a hypothesis for the oxidation of water via H_2O_3, we have not discounted other mechanistic routes that may depend on a concert of events that are unique to antibodies.

Given the conserved ability of antibodies (regardless of origin or antigen specificity) and of the αβTCR to mediate this reaction, x-ray structural studies were instigated to search for a possible conserved reaction site within these immunoglobulin fold proteins. A key constraint for any potential locus is that molecular oxygen (either $^1O_2$* or $^3O_2$ with a potential sensitizing residue, preferably Trp, in proximity) and water must be able to colocalize, and the transition states and intermediates along the pathway must be stabilized either within the site or in

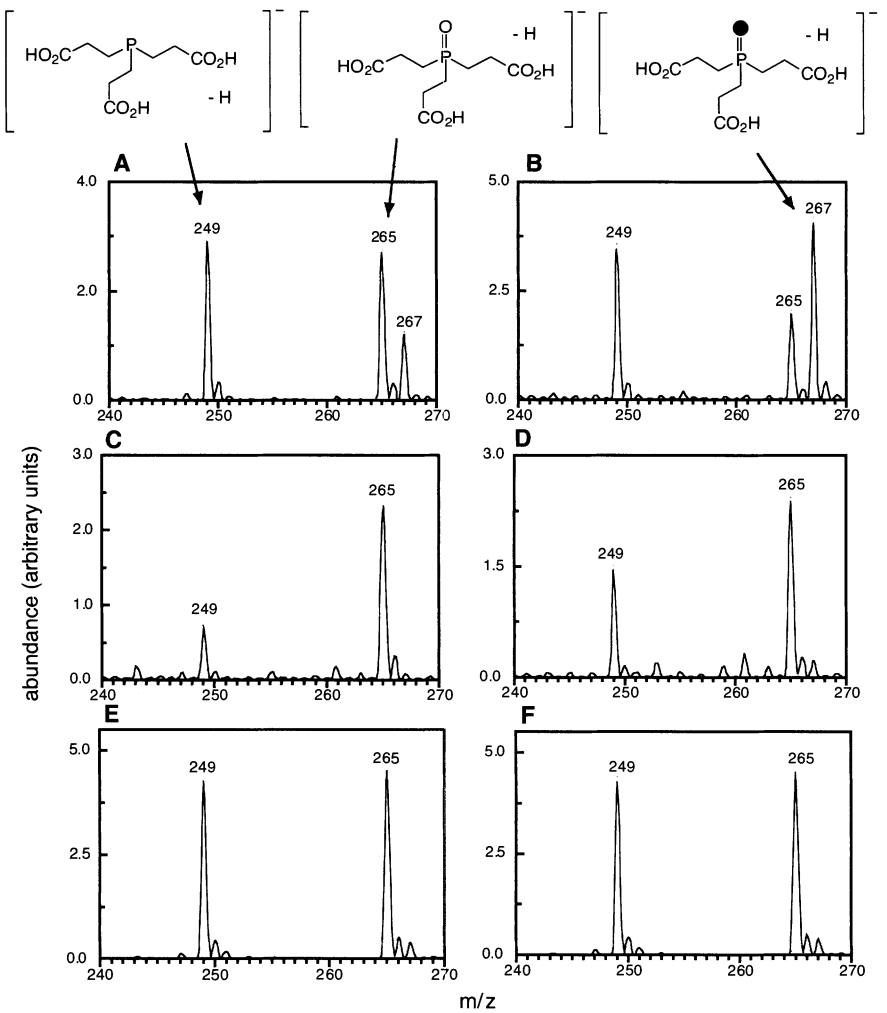

Fig. 5. Electrospray ionization (negative polarity) mass spectra of TCEP [$(M\text{-}H)^-$ 249] and its oxide [$(M\text{-}H)^-$ 265 (^{16}O) and $(M\text{-}H)^-$ 267 (^{18}O)] produced by oxidation with H_2O_2 [see (*7*) for assay conditions]. (**A**) After irradiation of sheep polyIgG (6.7 μM) under $^{16}O_2$ aerobic conditions in $H_2{}^{18}O$ (98% ^{18}O) PB. (**B**) After irradiation of sheep polyIgG (6.7 μM) under enriched $^{18}O_2$ (90% ^{18}O) aerobic conditions in $H_2{}^{16}O$ PB (*16*). (**C**) After irradiation of sheep polyIgG under $^{16}O_2$ aerobic concentration in $H_2{}^{16}O$ PB. In this assay, $H_2{}^{16}O$ replaced $H_2{}^{18}O$. (**D**) After irradiation of sheep polyIgG (6.7 μM) and $H_2{}^{16}O_2$ (200 μM) under anaerobic (degassed under argon) conditions in $H_2{}^{18}O$ PB for 8 hours at 20°C. (**E**) After irradiation of 3-methylindole (500 μM) under $^{16}O_2$ aerobic conditions in $H_2{}^{18}O$ PB. Size-exclusion filtration was not performed because of the low molecular weight of 3-methylindole. TCEP was added to the 3-methylindole–containing PB solution. (**F**) After irradiation of β-gal (50 μM) under $^{16}O_2$ aerobic conditions in $H_2{}^{18}O$ PB.

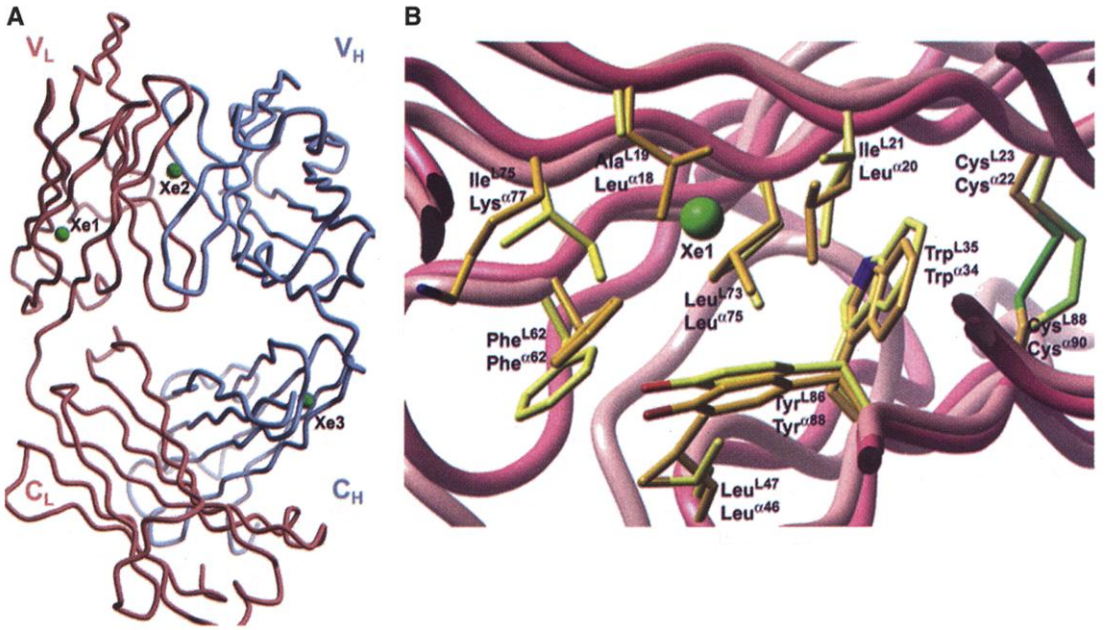

Fig. 6. The Xe binding sites in antibody 4C6 (*7*). (**A**) Standard side view of the C_α trace of Fab 4C6, with the light chain in pink and the heavy chain in blue. Three bound xenon atoms (green) are shown with the initial $F_{obs} - F_{calc}$ electron density map contoured at 5σ. (**B**) Overlay of Fab 4C6 and the 2C αβTCR (1TCR) around the conserved Xe1 site. The backbone C_α trace of V_L (pink) and side chains (yellow) and the corresponding V_α of the 2C αβTCR (red and gold) are superimposed. (Figure was generated with Insight 2000.)

close proximity. Xenon gas was used as a heavy-atom tracer to locate cavities within the murine monoclonal antibody 4C6 (*5, 7*) that may be accessible to O_2 (*29–31*). Three xenon sites (Xe1, Xe2, and Xe3) were identified (Fig. 6A), and all occupy hydrophobic cavities, as observed in other Xe-binding sites in proteins (*32, 33*). Superposition of the refined native and Xe-derivatized structures shows that, aside from addition of Xe, there is little discernible change in the protein backbone or side-chain conformation or in the location of bound water molecules.

The Xe1 site is conserved in all of the antibodies we studied and the αβTCR (Fig. 6B). Xe1 is in the middle of a highly conserved region between the β sheets of V_L (the variable region of immunoglobulin light chain), 7 Å from an invariant Trp. The Xe1 site is sandwiched between the two β sheets that constitute the immunoglobulin fold of the V_L, ~5 Å from the outside molecular surface. Xe2 sits at the base of the antigen binding pocket directly above several highly conserved residues that form the structurally conserved interface between the heavy and light chains of an antibody (Fig. 6A). The residues in the V_LV_H interface are primarily hydrophobic and include conserved aromatic side chains such as Trp^{H103}.

The contacting side chains for Xe1 in Fab 4C6 are Ala^{L19}, Ile^{L21}, Leu^{L73}, and Ile^{L75}, which are highly conserved aliphatic side chains in all antibodies; only slight structural variation was observed in this region in all antibodies surveyed. Notably, several other highly conserved and invariant residues are in the immediate vicinity of this xenon site, including Trp^{L35}, Phe^{L62}, Tyr^{L86}, Leu^{L104}, and the disulfide bridge between Cys^{L23} and Cys^{L88}. Trp^{L35} stacks against the disulfide bridge and is only 7 Å from the xenon atom. In this structural context, Trp^{L35} may be a putative molecular oxygen sensitizer, because it is the closest Trp to Xe1. Comparison with the 2C αβTCR structure (*3*) and all available TCR sequences shows that this Xe1 hydrophobic pocket is also highly conserved in TCRs (Fig. 6B). Thus, the xenon experiments have identified at least one site that is both accessible to molecular oxygen and is in a conserved region (V_L) in close proximity to an invariant Trp; an equivalent conserved site is also possible in the fold of V_H (*34*). Analysis of the sequence and structure around these sites shows that they are highly conserved in both antibodies and TCRs. This finding may provide a possible understanding of why the Ig fold in antibodies and the TCR can be involved in this unusual chemistry (*35*).

As discussed previously (*1*), antibody-catalyzed production of H_2O_2 from $^1O_2$* may participate in antibody-mediated cell killing by event-related production of H_2O_2. Alternatively, antibodies may function in defending an organism against $^1O_2$*. This postulate would require the further processing of H_2O_2 into water and $^3O_2$ by catalase (*36*). Because catalase is known to be an ancient protein arising as far back as archaebacteria (*37*), the question can be raised as to whether the structural element responsible for the catalytic destruction of $^1O_2$* is equally ancient and considerably precedes what we know today as antibodies. Singlet oxygen may even have played a decisive role in the initiation of the evolution of the immunoglobulin fold. Thus, it makes sense to search among ancient aerobic organisms for proteins that can accomplish similar chemistry.

References and Notes

1. A. D. Wentworth, L. H. Jones, P. Wentworth Jr., K. D. Janda, R. A. Lerner, *Proc. Natl. Acad. Sci. U.S.A.* **97**, 10930 (2000).
2. K. C. Garcia *et al.*, *Science* **274**, 209 (1996).
3. K. G. Welinder, H. M. Jespersen, J. W. Rasmussen, K. Skoedt, *Mol. Immunol.* **28**, 177 (1991).
4. T. Li, S. Hilton, K. D. Janda, *J. Am. Chem. Soc.* **117**, 3308 (1995).
5. This particular antibody was selected because its native crystals diffract to a higher resolution than any other published antibody (~1.3 Å). The root mean square differences (RMSDs) of key structural parameters were compared for the 4C6 structure before and after a soak experiment with 3 mM H_2O_2: RMSDs of all atoms, 0.412 Å; of Cα atoms, 0.327 Å; of main-chain atoms, 0.328 Å; of side-chain atoms, 0.488 Å.
6. F. Wilkinson, W. P. Helman, A. B. Ross, *J. Phys. Chem. Ref. Data* **22**, 113 (1993).
7. Experimental details of quantum efficiency of H_2O_2 production, Kabat database analysis, trace metal analysis, ^{18}O isotope incorporation, quantum chemical calculations, and crystallographic analyses are available on *Science* Online at www.sciencemag.org/cgi/content/full/293/5536/1806/DC1.
8. J. P. McCormick, T. Thomason, *J. Am. Chem. Soc.* **100**, 312 (1978).
9. P. Walrant, R. Santus, *Photochem. Photobiol.* **19**, 411 (1974).
10. A. V. Fowler, I. Zabin, *J. Biol. Chem.* **253**, 5521 (1978).
11. H. D. Scharf, R. Weitz, *Catal. Chem. Biochem. Theory Exp.* **12**, 355 (1979).
12. C. S. Foote, *Acc. Chem. Res.* **1**, 104 (1968).
13. J. Han, S. Yen, G. Han, P. Han, *Anal. Biochem.* **234**, 107 (1996).
14. In a typical experiment, a solution of sheep or horse polyIgG (6.7 μM, 100 μl) in PB (160 mM phosphate, pH 7.4) was degassed under an argon atmosphere for 30 min. This solution was then saturated with $^{18}O_2$ (90%) and assayed as described (*7*).
15. The reproducibility of the O^{16}/O^{18} ratio from protein samples lyophilized together is reasonable (±10%). However, problems with removing protein-bound water molecules during the lyophilization process means that the observed ratios can vary between samples from different lyophilization batches by as much as 2:1 to 4:1 (when lyophilizing from $H_2{}^{16}O$). It is therefore imperative that rigorous lyophilization and degassing procedures are followed. In this regard, the $^{18}O_2$ and $H_2{}^{16}O$ experiments exhibit less interassay variability because of the ease of removing protein-bound oxygen molecules.
16. Antibodies from different species give similar ratios within the experimental constraints detailed in (*15*). Observed ^{16}O:^{18}O ratios are as follows: WD1-6G6 mIgG (murine), 2.1:1; horse polyIgG, 2.2:1; sheep polyIgG, 2.2:1; EP2-19G2 mIgG (murine), 2.1:1; CH2-

5H7 mIgG (murine), 2.0:1; human polyIgG, 2.1:1. Ratios are based on means of duplicate determinations, except for horse polyIgG, which is the mean of 10 measurements (*7*).
17. Isotope experiments were also performed with β-galactosidase, the most efficient non-immunoglobulin protein at generating H_2O_2 (see above), as well as 3-methylindole. In both cases, photo-oxidation led to negligible ^{18}O incorporation into the H_2O_2 (Fig. 5, E and F, respectively), illustrating the view that the indole ring itself and tryptophan residues in this protein are behaving simply as reductants of $^1O_2$*. Irradiation of 3-methylindole generates H_2O_2 that does not include oxygen incorporation from $H_2{}^{18}O$. The same experiment performed with Trp gives rise to exchange with a $^{16}O/^{18}O$ ratio of 1.2:1. We attribute this result to the ammonium functionality acting as an intramolecular general acid that protonates the internal oxygen of a diastereomeric mixture of 3′-hydroperoxides. This process cannot account for the catalytic production of H_2O_2 by antibodies because it is stoichiometric.
18. D. R. Lide, *Handbook of Chemistry and Physics* (CRC Press, Boca Raton, FL, ed. 73, 1992).

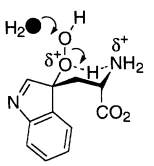

19. M. Detty, S. L. Gibson, *J. Am. Chem. Soc.* **112**, 4086 (1990).
20. C. Deby, *Recherche* **228**, 378 (1991).
21. D. T. Sawyer, *Oxygen Chemistry* (Oxford Univ. Press, Oxford, 1991).
22. J. Cerkovnik, B. Plesnicar, *J. Am. Chem. Soc.* **115**, 12169 (1993).
23. M. A. Vincent, I. A. Hillier, *J. Phys. Chem.* **99**, 3109 (1995).
24. B. Plesnicar, J. Cerkovnik, T. Tekavec, J. Koller, *Chem. Eur. J.* **6**, 809 (2000).
25. E. J. Corey, M. M. Mehrotra, A. U. Khan, *J. Am. Chem. Soc.* **108**, 2472 (1986).
26. J. Koller, B. Plesnicar, *J. Am. Chem. Soc.* **118**, 2470 (1996).
27. F. Cacace, G. de Petris, F. Pepi, A. Troiani, *Science* **285**, 81 (1999).
28. The complex problem of defining theoretically feasible reaction pathways for the conversion of H_2O_3 into H_2O_2, with or without the participation of $^1O_2$*, has been tackled in a systematic way using QC methods (B3LYP). This study revealed the existence of a whole spectrum of chemical pathways for the conversion of H_2O_3 to H_2O_2. Also, extensive docking calculations of H_2O_3 and the transition states for its formation and conversion into H_2O_2 have been investigated for a number of proteins (*38*).
29. Previous studies suggest that Xe and O_2 colocalize in the same cavities within proteins (*30, 31*).
30. R. F. Tilson Jr., U. C. Singh, I. D. Kuntz Jr., P. A. Kollman, *J. Mol. Biol.* **199**, 195 (1988).
31. B. P. Schoenborn, H. C. Watson, J. C. Kendrew, *Nature* **207**, 28 (1965).
32. E. E. Scott, Q. H. Gibson, *Biochemistry* **36**, 11909 (1997).
33. T. Prangé *et al.*, *Proteins Struct. Funct. Genet.* **30**, 61 (1998).
34. The structure and sequence around the Xe1 site is almost exactly reproduced in the V_H domain by the pseudo-twofold rotation axis that relates V_L to V_H. Although we did not locate a Xe binding site in this domain, O_2 could still access the corresponding cavity in V_H. The proposed heavy-chain Xe site may not have been found because the crystals were pressurized for only 2 min, due to Xe being too large compared to O_2 for the corresponding cavity on the V_H side, or because of crystal packing. In other antibody experiments, Xe binding sites were found in only one of the two molecules of the asymmetric unit, which suggests that crystal packing can modulate access of Xe in crystals.
35. Human β_2-microglobulin, which does not generate H_2O_2 (see above), does not have the same detailed structural characteristics that define the antibody Xe1 binding pocket, despite its overall immunoglobulin fold. Also, β_2-microglobulin does not contain the conserved Trp residue that occurs there in both antibodies and TCRs. If Trp^{L35} (antibodies) or $Trp^{\alpha 34}$ (TCR) is the oxygen sensitizer, the lack of a corresponding Trp in β_2-microglobulin may relate to the finding that it does not catalyze the oxidation of water.
36. For such a protection mechanism to be effective, catalase must not generate $^1O_2$* during H_2O_2 destruction. Currently, there is conflicting evidence regarding $^1O_2$* generation from catalase-mediated decomposition of H_2O_2 [see (*39*)].
37. V. Cannac-Caffrey *et al.*, *Biochimie* **80**, 1003 (1998).
38. D. Datta, X. Xu, N. Vaidehi, W. A. Goddard III, unpublished data.
39. J. R. Kanowsky, *Chem. Biol. Interact.* **70**, 1 (1989).
40. M. Zhou, Z. Diwu, N. Panchuk-Voloshina, R. P. Haugland, *Anal. Biochem.* **253**, 162 (1997).
41. Any concerns that the Amplex Red assay may be detecting protein-hydroperoxide derivatives in addition to H_2O_2 have been discounted, because the apparent H_2O_2 concentration measured using this method is independent of whether irradiated protein is removed from the sample (by size-exclusion filtration).
42. We thank members of the Scripps Research Institute mass spectroscopy facility, especially G. Suizdak and M. Sonderegger, for assistance with the isotope analysis; L. Teyton for the 2C TCRαβ; M. Pique for Kabat database analysis; K. Quon for ICP-AES antibody analyses; B. Zhou for mutagenesis studies; P. G. Schultz for helpful discussions; D. Datta, N. Vaidehi, R. P. Muller, and D. Chakraborty for stimulating discussions; and several Wilson lab members for help with data collection and processing, especially X. Daio. Supported by NIH grants GM43858 (K.D.J.), CA27489 (program project grant; K.D.J., I.A.W., R.A.L.), and HD 36385 (W.A.G.).

16 May 2001; accepted 12 July 2001

The Role of Atomic Ensembles in the Reactivity of Bimetallic Electrocatalysts

F. Maroun,* F. Ozanam,† O. M. Magnussen,‡ R. J. Behm

Bimetallic electrodes are used in a number of electrochemical processes, but the role of particular arrangements of surface metal atoms (ensembles) has not been studied directly. We have evaluated the electrochemical/catalytic properties of defined atomic ensembles in atomically flat PdAu(111) electrodes with variable surface stoichiometry that were prepared by controlled electrodeposition on Au(111). These properties are derived from infrared spectroscopic and voltammetric data obtained for electrode surfaces for which the concentration and distribution of the respective metal atoms are determined in situ by atomic resolution scanning tunneling microscopy with chemical contrast. Palladium monomers are identified as the smallest ensemble ("critical ensemble") for carbon monoxide adsorption and oxidation, whereas hydrogen adsorption requires at least palladium dimers.

Electrocatalytic reactions are of central importance in electrochemistry and play a vital role in emerging technologies related to environmental and energy-related applications, such as fuel cells. The efficiency and selectivity of electrocatalytic processes can be substantially improved by replacing monometallic with bimetallic catalysts. For example, the standard Pt electrocatalysts in polymer electrolyte membrane fuel cells are now being replaced by PtRu and PtMo alloys. The development of these bimetallic catalysts has been based primarily on empirical grounds. However, a detailed knowledge of the physical origins underlying the improvements in catalytic performance has been lacking so far.

Three explanations have been put forward for the higher activity of bimetallic catalysts: (i) Each metal component could promote different elementary reaction steps, leading to a "bifunctional mechanism" (*1*). (ii) Electronic effects resulting from interactions between the two metals could improve reactivity (*2*). (iii) The concept of geometric ensemble effects (specific groupings of surface atoms are required to serve as active sites), developed in heterogeneous gas-phase catalysis (*3*), has also been suggested for electrocatalysis (*4*). However, the direct experimental verification or quantitative assessment of the relative contributions of these effects has not been possible up to now. The lack of data on the local atomic arrangement at the surface, both for

Abteilung Oberflächenchemie und Katalyse, Universität Ulm, D–89069 Ulm, Germany.

*Present address: Laboratoire de Physique des Liquides et Electrochimie (CNRS UPR-15), Université P & M Curie, 4 Place Jussieu, F–75005 Paris, France.
†Permanent address: Laboratoire de Physique de la Matière Condensée, CNRS–Ecole Polytechnique, F-91128 Palaiseau, France.
‡To whom correspondence should be addressed. E-mail: olaf.magnussen@chemie.uni-ulm.de (O.M.M.); juergen.behm@chemie.uni-ulm.de (R.J.B.)